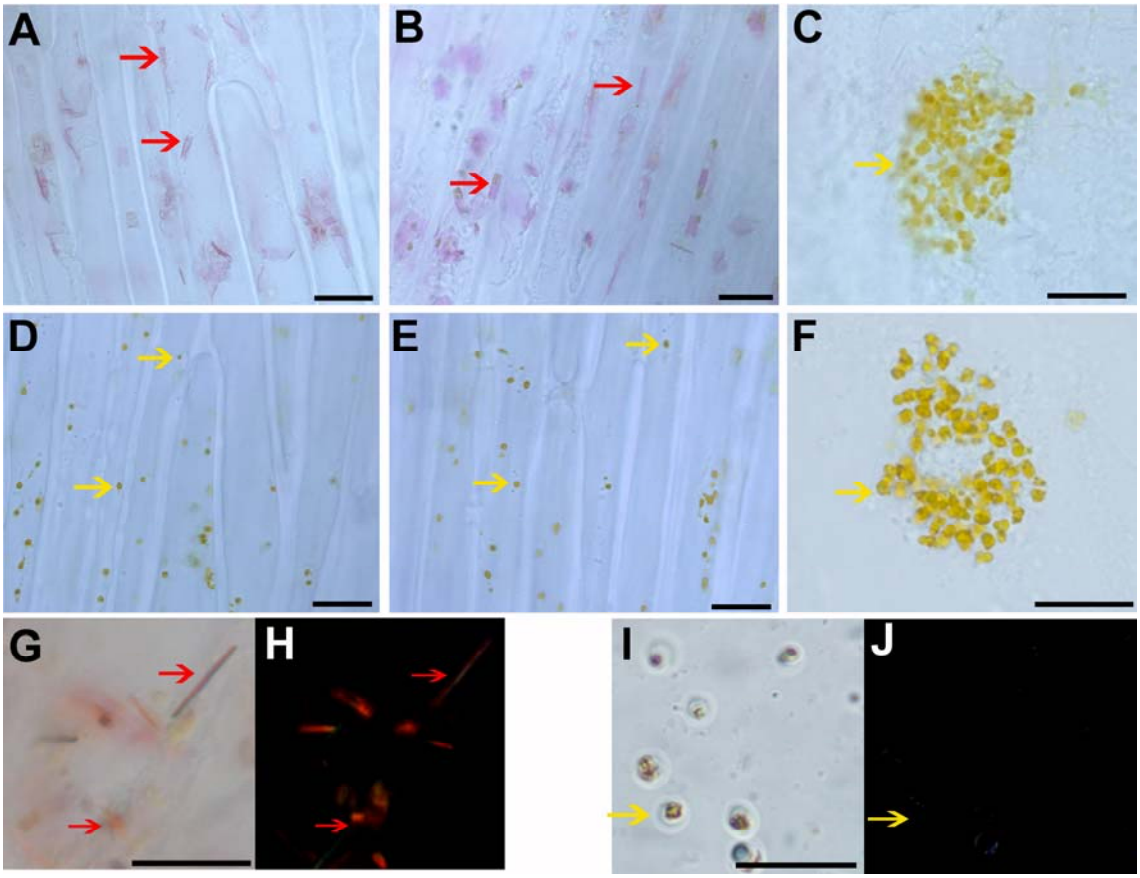

Supplemental Figure S1. Structural diversity of chromoplasts from the flesh of 'Cara Cara' and 'Newhall' Navel. Light microscopic inspection of the sac membrane, segment membrane, and juice that were separated from 'Cara Cara' **(A to C)** and 'Newhall' Navel **(D to F)** under normal light field microscopy. **G and H,** Carotenoid crystals within crystalloid chromoplasts confirmed by polarization microscopy in sac membrane and segment membrane of 'Cara Cara'. **I and J,** Polarization micrographs of globular chromoplasts in the flesh and juice of 'Newhall' Navel. Red- and yellow-arrows indicate crystalloid chromoplasts and globular chromoplasts, respectively. The bars represent 10 μm.

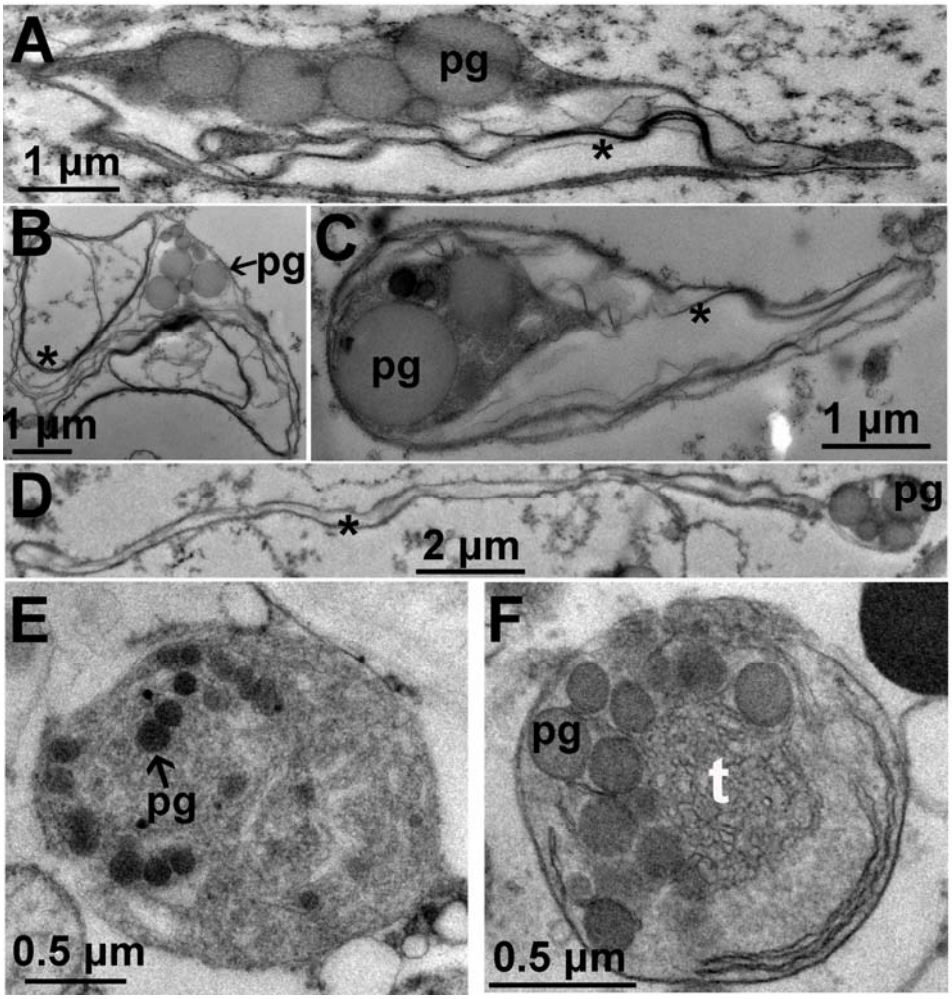

Supplemental Figure S2. Ultrastructures of chromoplasts from the flesh of 'Cara Cara' and 'Newhall' Navel. **A to D,** Ultrastructural diversity of crystalloid chromoplasts from segment membrane and sac membrane of 'Cara Cara'. Globular chromoplasts containing numerous plastoglobules were observed in juice of 'Cara Cara' **(E)** and 'Newhall' Navel flesh **(F)**. 'pg' denotes plastoglobules; '*' crystal remnants; 't' tubular structure.

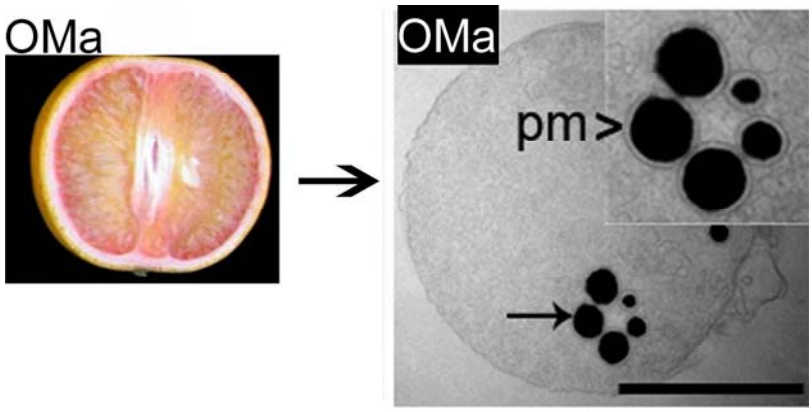

Supplemental Figure S3. The outer monolayer of plastoglobules appeared to be separated from the internal body at OMa stage. The ultrastructure of globular chromoplast of the juice in 'Hong Anliu' at OMa stage. The bar represents 2 μm.

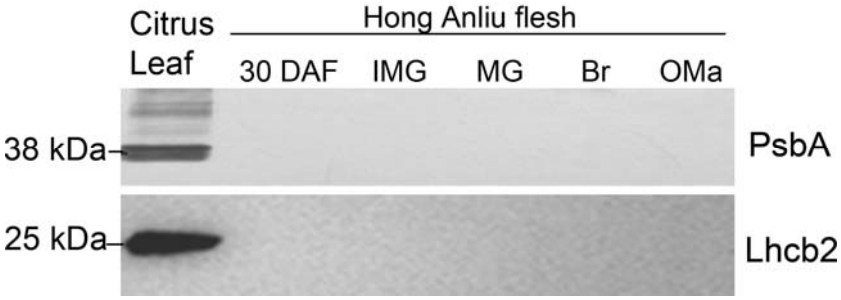

Supplemental Figure S4. Immunoblotting analysis reveals the absence of chloroplasts within citrus flesh during fruit maturity. Total proteins extracted from 'Hong Anliu' leaves (as control) or flesh at five different sampling points were subjected to gel blotting using antibodies against thylakoid membrane marker proteins (PsbA and Lhcb2). The same weight of proteins were used as loading control. At least two experimental replicates were conducted for immunoblotting analysis.

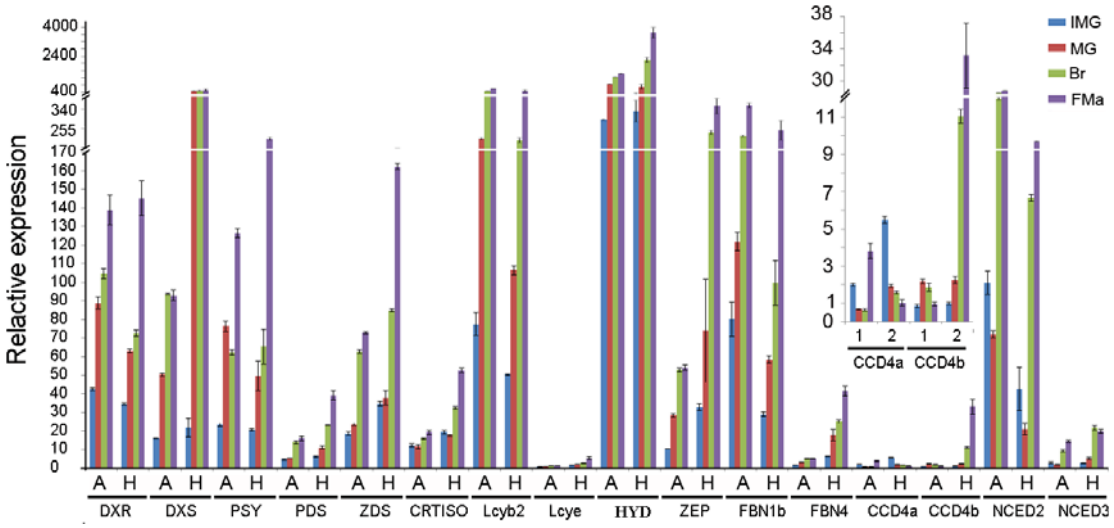

Supplemental Figure S5. Expression of carotenoid metabolic genes during the formation of chromoplasts at different maturation stages. Relative transcript levels were analysed by real-time RT-PCR in the segment membrane of 'Anliu' (A) and 'Hong Anliu' (H). Data represent mean values ± SD from at least three experimental replicates. The expression levels of Actin were used to normalize the expression for each sample.

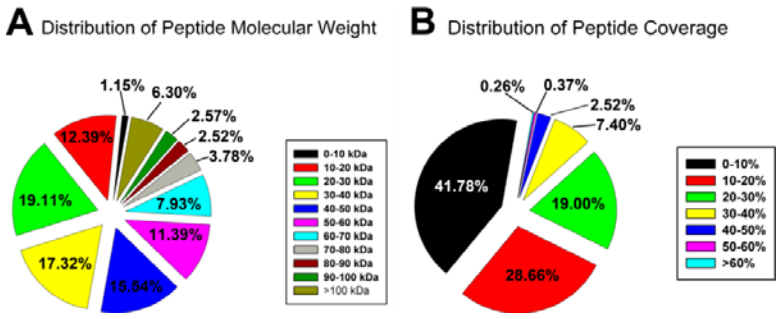

Supplemental Figure S6. Distribution of peptide molecular weight **(A)** and of peptide coverage **(B).**

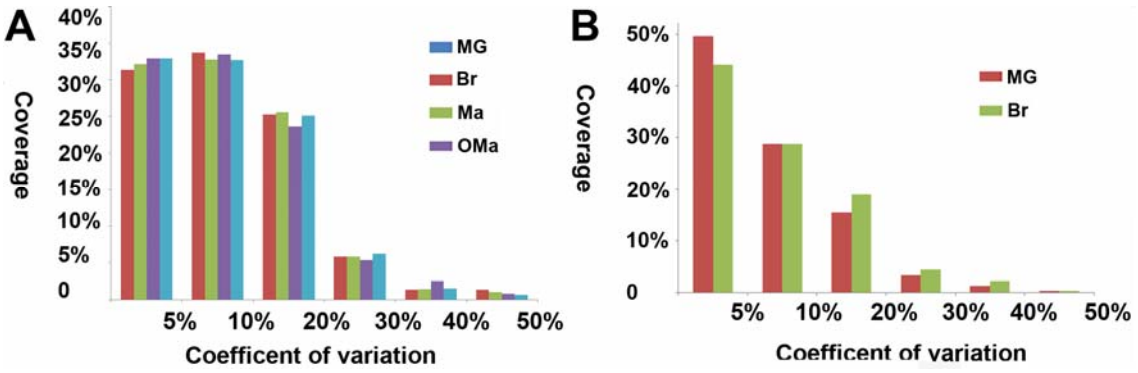

Supplemental Figure S7. Analysis of reproducibility of iTRAQ biological replicates and technological replicates of each development stage. **A,** Reproducibility of biological replicates (MG-1_E1_114 VS MG-2_E1_119 VS MG-3_E2_115; Br-1_E1_117 VS Br-2_E1_121 VS Br-3_E2_114; Ma-1_E1_116 VS Ma-2_E2_118 VS Ma-3_E2_121; OMa-1_E1_115 VS OMa-2_E1_118 VS OMa-3_E2_117 as showed in Figure 7). **B,** Reproducibility of technological replicates (MG-3_E2_115 VS MG-4_E2_116 and Br-1_E1_117 VS Br-2_E1_121).

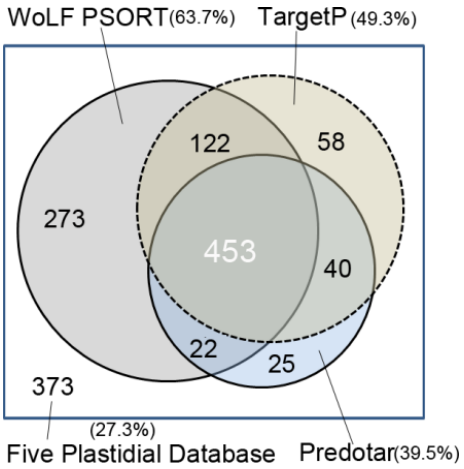

Supplemental Figure S8. Venn diagram of the number of proteins of the citrus plastid proteome predicted to be plastid localized by three predictors and five plastidial databases. A total of 1,366 proteins are predicted by at least one predictor or more than two out of five plastidial databases. The 20 plastid-genome encoded proteins were excluded from this analysis.

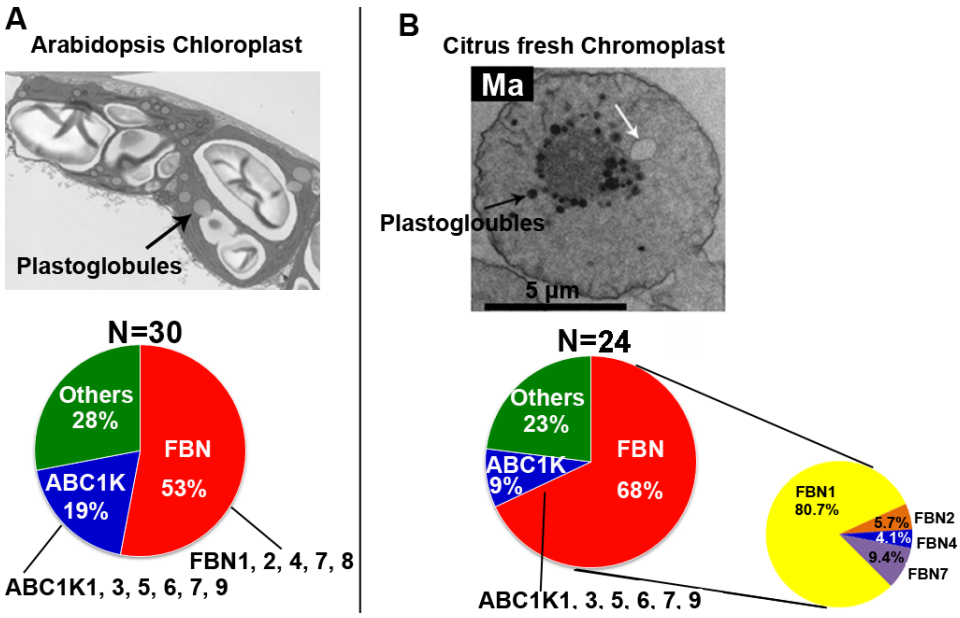

Supplemental Figure S9. Relative mass contributions of the 30 plastoglobule core proteins to the total core plastoglobule proteome for Arabidopsis chloroplasts **(A)** and orange flesh chromoplasts **(B)**. The graph of Arabidopsis cellular ultrastructure and plastoglobule-localized proteins was taken from the study by Lundquist et al. (2012).

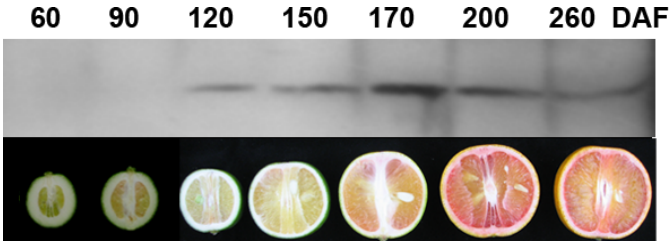

Supplemental Figure S10. Abundance of FBN1 during fruit ripening. 30 μg of total proteins extracted from 'Hong Anliu' fruit from 60 DAF to 260 DAF were separated using SDS-PAGE, blotted and subjected to immunoassays using FBN1 antibodies. The equal amount of proteins was performed as a loading control.